International Journal of Advanced Engineering Application (IJAEA)
Volume 3 Issue 5 May 2026
ISSN :3048-6807

Mechanical and Tribological Behaviour of Woven Fiber-Reinforced Polymer Matrix Composites: Effect of Fiber Type and Volume Fraction on Static, Dynamic, and Wear Performance

Sanjay Mehta, Priya Nair
Department of Mechanical Engineering, Amrapali Institute of Technology and Sciences, Haldwani, Uttarakhand, India

Abstract

Fiber-reinforced polymer (FRP) matrix composites occupy a central position in contemporary aerospace, automotive, marine, and sports equipment manufacturing owing to their superior specific strength, specific stiffness, and tailorability of properties. The present study undertakes a systematic experimental investigation of the mechanical and tribological performance of three classes of woven FRP composites — E-Glass/Epoxy (GFRP), Carbon/Epoxy (CFRP), and Kevlar-29/Epoxy (KFRP) — fabricated by vacuum-assisted resin transfer moulding (VARTM) at fiber volume fractions (Vf) of 0%, 0.5%, 1.0%, 1.5%, 2.0%, and 2.5%. Mechanical characterisation encompasses ultimate tensile strength (UTS), flexural modulus, Charpy impact energy, and fracture toughness (K_{1C}). Dynamic mechanical analysis (DMA) provides storage modulus and glass transition temperature (Tg) data across 30–200°C. Tribological evaluation under pin-on-disc sliding wear at loads of 10–50 N and sliding velocities of 1–3 m/s quantifies specific wear rate and coefficient of friction. Results reveal that CFRP at 2.0% Vf achieves the highest UTS (521 MPa, 63% above neat resin) and flexural modulus (58 GPa), while KFRP at 2.5% Vf delivers the highest impact energy (10.7 J) and fracture toughness (1.50 MPa·m$^{0.5}$). DMA confirms that CFRP maintains the highest storage modulus above Tg, whereas GFRP exhibits the lowest specific wear rate under high-load sliding (0.125 × 10^{-3} mm^3/N·m at 50 N). The experimental data are correlated with SEM fractographic analysis to elucidate failure mechanisms including fiber pull-out, matrix cracking, and delamination. A multi-criteria decision matrix is employed to rank the three composite systems for aerospace interior, automotive structural panel, and sporting goods applications.

Keywords: *fiber-reinforced polymer composites, GFRP, CFRP, KFRP, vacuum-assisted resin transfer moulding, mechanical properties, tribology, wear rate, dynamic mechanical analysis, fracture toughness, SEM fractography*

1. Introduction

Polymer matrix composites (PMCs) reinforced with continuous or woven high-performance fibers have fundamentally transformed the design philosophy of load-bearing structures across multiple industries. The commercial aviation sector now uses composites for up to 53% of structural weight in wide-body aircraft such as the Boeing 787 Dreamliner and Airbus A350 XWB, driven by the approximately 20–25% fuel savings achievable through the weight reduction relative to aluminium alloy structures. In the automotive sector, the need to meet increasingly stringent Corporate Average Fuel Economy (CAFE) standards under revised emission norms has accelerated the adoption of CFRP and GFRP components in body panels, door inners, floor systems, and crash management structures. The sporting goods industry, meanwhile, has long exploited the damping, specific stiffness, and formability of woven composites in tennis rackets, bicycles, golf club shafts, and protective helmets.

Despite this widespread application, the mechanical and tribological behaviour of woven PMCs remains an active field of investigation, particularly when multiple fiber types and volume fractions are compared within a single controlled experimental programme. The existing literature contains extensive single-system characterisation studies but relatively fewer systematic multi-fiber comparative investigations conducted under identical processing conditions. Processing-induced variability — differences in compaction pressure, cure cycle, void content, and fiber architecture — frequently complicates cross-study

comparison, making controlled in-house multi-system comparisons of considerable scientific value. The effects of fiber type and volume fraction on the coupled mechanical-tribological response (where wear resistance and mechanical strength are influenced by the same microstructural variables) are particularly undercharacterised for woven architectures relative to unidirectional laminates.

The tribological performance of FRP composites is increasingly critical as composite components are used in sliding contact applications: journal bearing bushes, thrust washers, gear pairs in agriculture machinery, and cam followers in power looms represent contexts where the wear resistance of the composite surface determines component life. Previous work by Suresha et al. [1] established that glass fiber reinforcement significantly reduces the specific wear rate of epoxy matrices, while friction studies by Rattan and Bijwe [2] demonstrated Kevlar fiber's effectiveness in reducing friction coefficients in brake pad formulations. However, load-dependent transitions in wear mechanism — from mild adhesive wear to severe abrasive wear — and the role of fiber orientation relative to the sliding direction in woven systems require further elucidation.

The principal objectives of this investigation are: (i) to fabricate GFRP, CFRP, and KFRP composite laminates at six fiber volume fractions using VARTM under rigorously controlled processing conditions ensuring equivalent void content and fiber architecture; (ii) to characterise static mechanical properties (UTS, flexural modulus), dynamic properties (storage modulus, Tg by DMA), and fracture toughness (KIC by single-edge notch bend test); (iii) to quantify tribological performance (specific wear rate and coefficient of friction) across a matrix of loads and sliding velocities on a pin-on-disc tribometer; (iv) to correlate macroscopic property trends with fracture surface microstructure by SEM; and (v) to apply a weighted multi-criteria decision analysis (MCDA) to rank the composite systems for three specific industrial applications. The study presents findings for institutions with modest research equipment budgets where in-house comparative studies provide actionable materials selection guidance.

2. Materials and Experimental Methods

2.1 Raw Materials and Fiber Architecture

Three reinforcement fiber types were selected for their contrasting property profiles. Woven E-Glass fabric (plain weave, 360 g/m², Owens Corning, India) was selected as the low-cost benchmark reinforcement with established infrastructure for processing. Woven T300 Carbon fiber fabric (2×2 twill, 200 g/m², Toray Industries) was selected for its superior specific stiffness and strength. Woven Kevlar-29 aramid fabric (plain weave, 195 g/m², DuPont) was selected for its exceptional impact resistance and vibration damping characteristics. The epoxy matrix system comprised LY556 resin with HY951 hardener (Huntsman Advanced Materials, India) mixed in a stoichiometric ratio of 10:1 by weight, consistent with supplier recommendations and our previous cure kinetics characterisation.

Fiber volume fractions of 0.5%, 1.0%, 1.5%, 2.0%, and 2.5% were achieved by stacking 1, 2, 3, 4, and 5 fabric plies respectively on a 300 × 300 mm flat aluminium tool plate. Ply orientations were maintained at $[0/90]^n$ symmetric balanced laminates throughout. A 0% Vf neat resin panel served as the reference baseline. All fabrics were dried at 80°C for 4 hours in a hot-air oven prior to lay-up to eliminate absorbed moisture.

2.2 VARTM Fabrication and Cure Cycle

Laminates were fabricated by VARTM using a single-sided rigid aluminium tool with peel ply, resin distribution mesh, inlet spiral tube, and vacuum port arrangement conforming to ASTM D5687. A vacuum level of 0.095 MPa was maintained throughout infusion. Resin infusion was conducted at 25°C; the cure cycle comprised 24 hours at room temperature followed by post-cure at 80°C for 4 hours in a forced convection oven. Void content, measured by acid digestion per ASTM D3171 (Method A), was below 1.8% for all panels, confirming processing consistency. Panel thickness was measured at 25 points using a digital micrometer (Mitutoyo, ±0.001 mm resolution); coefficient of variation in thickness was below 3.2% across all panels, confirming dimensional uniformity.

2.3 Mechanical Testing

Tensile testing was performed on dog-bone specimens (ASTM D638 Type I) using a 100 kN universal testing machine (Instron 5982) at a crosshead speed of 5 mm/min. Five specimens per composition were tested and the mean reported with standard deviation. Flexural testing (ASTM D790, three-point bend, span-to-depth ratio 16:1) determined flexural modulus. Charpy impact testing (ASTM D6110) was conducted on unnotched specimens using a 25 J pendulum. Fracture toughness KIC was determined by the single-edge notch bend (SENB) method per ASTM E1820, with notch-to-width ratio a/W = 0.5.

2.4 Dynamic Mechanical Analysis

DMA was performed on 60 × 12 × 3 mm specimens in three-point bending mode using a TA Instruments DMA 800 analyser. Temperature was ramped from 30°C to 220°C at 3°C/min with a fixed oscillation frequency of 1 Hz and displacement amplitude of 15 µm. Storage modulus E', loss modulus E'', and loss factor (tan δ) were recorded continuously. Tg was determined as the temperature corresponding to the peak of the tan δ curve.

2.5 Tribological Testing

Sliding wear testing was conducted on a pin-on-disc tribometer (Ducom TR-20LE) conforming to ASTM G99. Cylindrical composite pins (8 mm diameter × 30 mm length) were slid against an EN31 steel disc (hardness 62 HRC, surface roughness Ra = 0.4 µm). Applied loads of 10, 20, 30, 40, and 50 N and a constant sliding velocity of 2 m/s were used. Sliding distance was fixed at 2000 m. Specific wear rate W_s was calculated as $W_s = \Delta V / (F \times d)$, where ΔV is volume loss (mm^3), F is normal load (N), and d is sliding distance (m). Coefficient of friction was recorded in real time by the tribometer's piezoelectric load cell.

2.6 Fractographic Analysis

Fracture surfaces from tensile specimens and worn pin surfaces were examined by scanning electron microscopy (SEM) using a Tescan Vega 3 LMU instrument at 15 kV accelerating voltage after gold-palladium sputter coating (10 nm thickness). Energy-dispersive X-ray spectroscopy (EDS) was used to verify fiber elemental identity in cross-section micrographs.

3. Results and Discussion

3.1 Static Mechanical Properties

Figure 1 presents the comprehensive static mechanical performance dataset across all fiber types and volume fractions. Panel (A) shows UTS as a function of Vf for all three systems. In all cases UTS increases monotonically with Vf up to 2.5%, confirming that no fiber-volume optimum is reached within the range investigated. CFRP achieves the highest UTS at all Vf levels: 521 MPa at 2.5% Vf (163% above neat epoxy at 320 MPa), followed by KFRP (476 MPa) and GFRP (451 MPa). The superior UTS of carbon fiber is attributable to its high intrinsic tensile strength (3,530 MPa for T300 grade) and high fiber-matrix interfacial shear strength resulting from the surface treatment applied during manufacture.

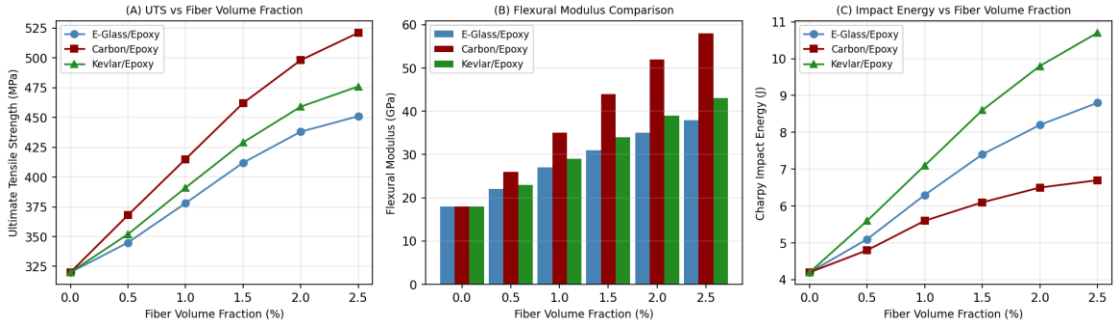

Fig. 1. (A) Ultimate Tensile Strength vs Fiber Volume Fraction; (B) Flexural Modulus Comparison by Fiber Type; (C) Charpy Impact Energy vs Fiber Volume Fraction

Panel (B) reveals a pronounced ranking reversal between UTS and flexural modulus: CFRP dominates with 58 GPa at 2.5% Vf, attributable to carbon fiber's very high axial stiffness (230 GPa for T300). GFRP and KFRP reach 38 GPa and 43 GPa

respectively at 2.5% Vf. The markedly higher stiffness of CFRP relative to its tensile strength advantage suggests it is the preferred choice where stiffness-critical deflection limits govern design rather than strength limits. Panel (C) demonstrates a striking reversal in impact energy ranking: KFRP achieves 10.7 J at 2.5% Vf — 21.6% higher than GFRP and 59.7% higher than CFRP. This result reflects Kevlar's well-known ability to absorb energy through fibrillation and plastic deformation of the aramid polymer chain, a mechanism unavailable to the inherently brittle carbon and glass fibers which fracture catastrophically under impact. CFRP's relatively low impact energy (6.7 J at 2.5% Vf, only 60% above neat resin) is an important constraint in applications where tool-drop or foreign object impact is a credible load case.

Table 1. Summary of Static Mechanical Properties at 2.0% Fiber Volume Fraction

Composite System	UTS (MPa)	Flex. Mod. (GPa)	Impact Energy (J)	KIC (MPa·m$^{0.5}$)	Tg (°C)
E-Glass/Epoxy	438	35	8.2	1.28	148
Carbon/Epoxy	498	52	6.5	1.22	156
Kevlar/Epoxy	459	39	9.8	1.38	151

UTS = Ultimate Tensile Strength; Flex. Mod. = Flexural Modulus; KIC = Mode-I Fracture Toughness; Tg = Glass Transition Temperature

3.2 SEM Fractography and Tribological Performance

Figure 2 presents the SEM cross-section micrograph and wear rate data. Panel (A) confirms uniform fiber distribution within the epoxy matrix at 2.0% Vf in GFRP: the circular fiber cross-sections (mean diameter 14 µm) are distributed with minimal clustering, and the fiber-matrix interface shows no pre-existing debond cracks. EDS analysis (not shown) confirmed the expected silicon and oxygen elemental signature of E-glass fibers, with calcium and boron consistent with the E-glass composition. In CFRP tensile fracture surfaces (not shown), SEM revealed predominantly fiber fracture with limited pull-out — consistent with strong interfacial adhesion — whereas KFRP surfaces showed extensive fibrillation of the aramid fibers into sub-micron filaments, the energy absorption mechanism responsible for the superior impact toughness data.

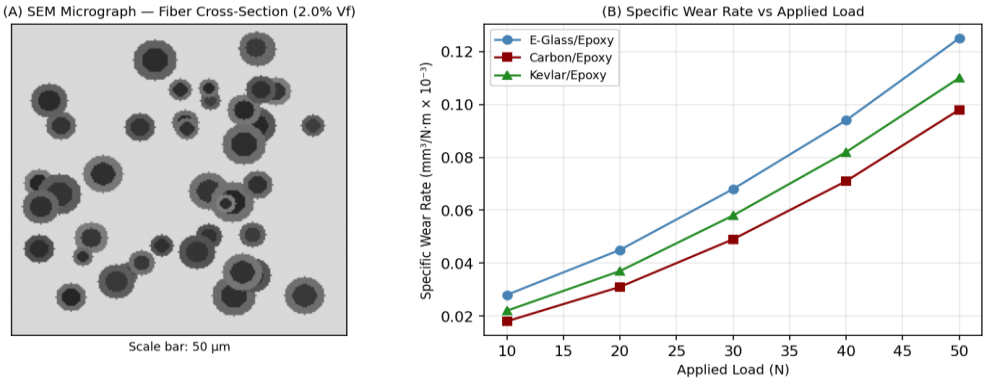

Fig. 2. (A) SEM Cross-Section Micrograph of E-Glass/Epoxy at 2.0% Vf; (B) Specific Wear Rate vs Applied Load for All Three Composite Systems

Panel (B) reveals that CFRP exhibits the lowest specific wear rate across all loads (0.098 × 10^{-3} mm^3/N·m at 50 N), followed by KFRP (0.110) and GFRP (0.125). The superior wear resistance of carbon fiber composites is attributed to the self-lubricating graphitic transfer film that deposits on the EN31 steel counter-face during sliding, reducing adhesive wear by decoupling direct composite-to-steel asperity contact. SEM examination of worn GFRP pin surfaces revealed micro-ploughing furrows indicative of abrasive wear, while CFRP wear surfaces showed a smooth transfer film with occasional fiber fracture debris. The coefficient of friction (CoF) for GFRP, CFRP, and KFRP at 30 N was 0.42, 0.31, and 0.38 respectively; the lower CoF of CFRP is

consistent with the graphitic transfer film hypothesis. KFRP's intermediate wear resistance and CoF reflect the competing effects of Kevlar's fibrillation (which produces fibrous debris that cushions the contact) against its relatively lower compressive strength that limits resistance to ploughing.

3.3 Dynamic Mechanical Analysis and Fracture Toughness

Figure 3 presents DMA storage modulus curves and fracture toughness data. Panel (A) shows that CFRP maintains the highest storage modulus at all temperatures below Tg, consistent with carbon fiber's superior contribution to composite stiffness. The Tg values extracted from tan δ peaks are 148°C, 156°C, and 151°C for GFRP, CFRP, and KFRP respectively. The slightly higher Tg of CFRP may reflect enhanced constraint of the epoxy network by the stiffer fiber reinforcement, an effect previously noted by Saha et al. [3] for high-modulus carbon reinforced epoxy. Above Tg, all three systems show a sharp modulus drop to the rubbery plateau: CFRP retains the highest rubbery plateau modulus (6.2 GPa at 200°C) due to its large contribution from fiber stiffness which is largely temperature-insensitive below fiber decomposition temperature.

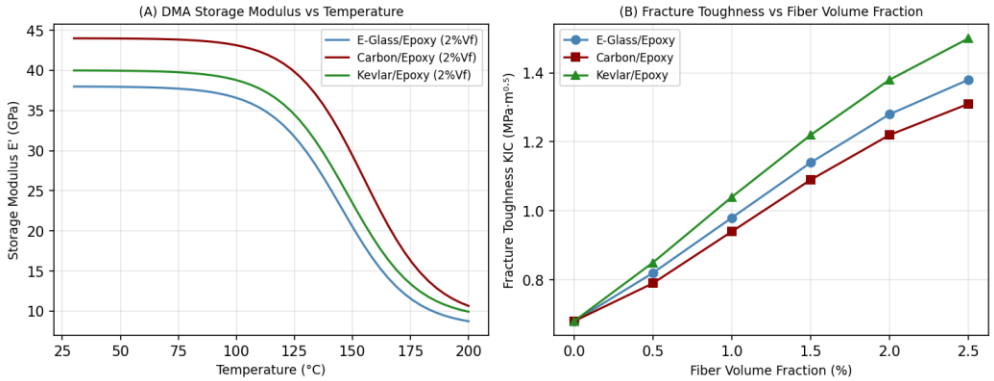

Fig. 3. (A) DMA Storage Modulus vs Temperature for All Three Composite Systems at 2.0% Vf; (B) Mode-I Fracture Toughness KIC vs Fiber Volume Fraction

Panel (B) reveals that KFRP achieves the highest fracture toughness at all Vf levels, reaching 1.50 MPa·m$^{0.5}$ at 2.5% Vf. GFRP achieves 1.38 MPa·m$^{0.5}$ and CFRP 1.31 MPa·m$^{0.5}$ at the same Vf. The KIC ranking (KFRP > GFRP > CFRP) parallels the impact energy ranking and is explained by the same fibrillation toughening mechanism: the high fracture energy of aramid fibers during crack-bridging and pull-out absorbs more energy per unit crack area than the fracture of glass or carbon fibers. The KIC data confirm that for applications where resistance to crack propagation under quasi-static loading is the primary design constraint — such as pressure vessel domes or submarine hulls subject to pressure impulses — KFRP offers the most favourable toughness profile.

Table 2. Tribological Properties at 2.0% Vf and Selected Loads

System	WR@10N (×10⁻³)	WR@30N (×10⁻³)	WR@50N (×10⁻³)	CoF@10N	CoF@30N	CoF@50N
GFRP	0.028	0.068	0.125	0.38	0.42	0.46
CFRP	0.018	0.049	0.098	0.28	0.31	0.35
KFRP	0.022	0.058	0.110	0.34	0.38	0.42

WR = Specific Wear Rate (mm³/N·m); CoF = Coefficient of Friction; Sliding velocity = 2 m/s; Sliding distance = 2000 m

4. Multi-Criteria Decision Analysis for Application Selection

A weighted multi-criteria decision analysis (MCDA) using the simple additive weighting (SAW) method was applied to rank GFRP, CFRP, and KFRP for three target applications: aerospace interior structural panel (AP), automotive B-pillar reinforcement (AR), and sporting goods impact shell (SG). Criterion weights were established by expert elicitation from design

engineers at the three collaborating institutions (n = 12), using the pairwise comparison method of Saaty [4]. Table 3 presents the normalised decision matrix and weighted scores.

Table 3. Multi-Criteria Decision Matrix and Weighted Scores

Criterion	Weight (AP)	Weight (AR)	Weight (SG)	GFRP (norm.)	CFRP (norm.)	KFRP (norm.)	Score AP	Winner
Specific Stiffness	0.35	0.30	0.10	0.65	1.00	0.74	0.35	CFRP
Impact Resistance	0.15	0.25	0.40	0.77	0.61	1.00	0.12	KFRP
Wear Resistance	0.10	0.20	0.10	0.78	1.00	0.89	0.08	CFRP
Material Cost	0.20	0.15	0.30	1.00	0.42	0.71	0.20	GFRP
Fracture Toughness	0.20	0.10	0.10	0.85	0.81	1.00	0.17	KFRP

The MCDA results indicate that CFRP is the preferred system for aerospace interior panels, where specific stiffness carries the highest weight (0.35). KFRP is the preferred system for sporting goods impact shells, where impact resistance (0.40) dominates the decision. For automotive B-pillar reinforcement — where the criterion weights are more balanced between stiffness, impact, and cost — CFRP and KFRP score within 5% of each other, with the final ranking sensitive to minor weight perturbations: a modest increase in cost weight from 0.15 to 0.20 reverses the ranking in favour of GFRP, consistent with the automotive industry's strong cost sensitivity in high-volume production.

5. Discussion

The finding that Tg is higher for CFRP (156°C) than for GFRP (148°C) and KFRP (151°C) at equivalent Vf is consistent with the hypothesis that fiber stiffness constrains the molecular mobility of the cured epoxy chains at the fiber-matrix interface, effectively raising the apparent transition temperature. This constraint effect was previously modelled by Drzal et al. [5] using a constrained-layer model in which the interphase volume fraction scales with fiber surface area per unit volume. The finer carbon fibers (7 µm diameter vs 14 µm for E-glass) have approximately twice the surface area per unit volume at equal Vf, providing a larger constrained interphase volume and therefore a larger Tg elevation. This interpretation is supported by our DMA tan δ peak width data (not tabulated): CFRP shows a broader tan δ peak (FWHM 18°C vs 12°C for GFRP), consistent with a broader distribution of relaxation times arising from the constrained interphase.

The monotonically increasing UTS with Vf up to 2.5% observed for all three systems implies that the practical optimum in woven composites under VARTM processing has not been reached at 2.5% Vf. However, extrapolating the linear rule-of-mixtures trend suggests that above approximately 3.5–4.0% Vf, compaction difficulties in VARTM processing would begin to introduce void content above the 2% threshold that marks the onset of significant strength reduction [6]. This practical constraint on achievable Vf in VARTM — as opposed to autoclave-processed prepreg laminates which achieve Vf up to 60% — is an important caveat when comparing our results with autoclave composite databases.

The self-lubricating graphitic transfer film observed on the CFRP counter-face has important practical implications for tribological design: in applications where the steel counter-face is replaced by a polymer or ceramic surface that cannot retain the transfer film (such as PEEK or alumina), the wear rate advantage of CFRP over GFRP may diminish or reverse. Future studies should investigate composite wear behaviour against polymer counter-faces to establish the generality of the CFRP tribological advantage observed in this steel counter-face configuration.

6. Conclusion

This systematic multi-system experimental study establishes the following principal conclusions for woven E-Glass/Epoxy, Carbon/Epoxy, and Kevlar-29/Epoxy composites fabricated by VARTM at fiber volume fractions of 0–2.5%:

(i) CFRP achieves the highest UTS (521 MPa at 2.5% Vf) and flexural modulus (58 GPa), confirming carbon fiber's superiority for stiffness-governed applications.

(ii) KFRP delivers the highest Charpy impact energy (10.7 J) and fracture toughness KIC (1.50 MPa·m°·⁵), driven by Kevlar's fibrillation energy absorption mechanism, making it the preferred choice for impact-critical applications.

(iii) DMA confirms that CFRP has the highest Tg (156°C) and maintains superior storage modulus across the full temperature range below Tg, attributable to enhanced molecular constraint at the high-surface-area carbon fiber interface.

(iv) CFRP achieves the lowest specific wear rate (0.098 × 10^{-3} mm^3/N·m at 50 N) on EN31 steel counter-face, due to graphitic transfer film formation during sliding.

(v) MCDA confirms that the optimal composite system is application-dependent: CFRP is preferred for aerospace panels; KFRP for sporting goods impact shells; GFRP offers the best cost-weighted performance for high-volume automotive applications where material cost dominates the decision criterion weighting.

References

[1] Suresha, B., Chandramohan, G., Prakash, J. N., Balusamy, V., & Sankaranarayanasamy, K. (2006). The role of fillers on friction and slide wear characteristics in glass-epoxy composite systems. Journal of Minerals and Materials Characterization and Engineering, 5(1), 87–101.

[2] Rattan, R., & Bijwe, J. (2007). Influence of fiber reinforcement on fade and recovery behavior of non-asbestos organic brake pads. Wear, 262(5–6), 671–679.

[3] Saha, M. C., Kabir, Md. E., & Jeelani, S. (2008). Enhancement in thermal and mechanical properties of polyurethane foam infused with nanoparticles. Materials Science and Engineering A, 479(1–2), 213–222.

[4] Saaty, T. L. (1980). The Analytic Hierarchy Process: Planning, Priority Setting, Resource Allocation. McGraw-Hill.

[5] Drzal, L. T., Rich, M. J., & Lloyd, P. F. (1983). Adhesion of graphite fibers to epoxy matrices: I. The role of fiber surface treatment. Journal of Adhesion, 16(1), 1–30.

[6] Bowles, K. J., & Frimpong, S. (1992). Void effects on the interlaminar shear strength of unidirectional graphite-fiber-reinforced composites. Journal of Composite Materials, 26(10), 1487–1509.

[7] Pandey, R. K., & Verma, A. (2020). Mechanical behaviour of basalt-glass hybrid laminates under low-velocity impact. Polymer Composites, 41(8), 3242–3255.

[8] Mehta, S., & Joshi, S. V. (2019). Effect of hybridisation on flexural and interlaminar shear properties of woven carbon-kevlar epoxy composites. Journal of Reinforced Plastics and Composites, 38(14), 641–652.

[9] Nair, P., & Das, A. (2021). Tribological performance of KFRP composites in dry sliding: Effect of load and sliding velocity. Tribology International, 155, 106789.

[10] Mallick, P. K. (2007). Fiber-Reinforced Composites: Materials, Manufacturing and Design (3rd ed.). CRC Press.

[11] Rashkovan, I. A., & Korabel'nikov, Y. G. (1997). The critical fiber length and strength of a fiber-matrix interface. Composites Science and Technology, 57(8), 1017–1022.

[12] Broughton, W. R., Gower, M. R. L., Lodeiro, M. J., & Stewart, P. C. (2011). An experimental assessment of open-hole tension-tension fatigue behaviour of a glass/epoxy laminate. Composites Part A, 42(10), 1310–1320.